JOURNAL OF APPLIED POLYMER SCIENCE VOL. 18, PP. 1053–1078 (1974)

Structure Development During Melt Spinning of Linear Polyethylene Fibers

J. R. DEES* and J. E. SPRUIELL, *Department of Chemical and Metallurgical Engineering, The University of Tennessee, Knoxville, Tennessee 37916*

Synopsis

Apparatus has been developed for studying the development of crystallinity and orientation during the melt spinning of synthetic fibers. Tension in the fiber and fiber temperature, diameter, and x-ray diffraction patterns are measured as a function of distance from the spinneret for a running monofilament. Measurements are presented for linear polyethylene over a range of spinning variables together with other investigations carried out on the final as-spun fibers. These data indicate that the development of crystallinity in polyethylene is controlled by a balance between increased crystallization kinetics caused by the stress in the fiber and a tendency for increased supercooling with change in any spinning variable that increases cooling rates in the fiber. The type of crystalline orientation observed, its development during the spinning process, and the changes observed with changes in spinning conditions suggest a model for the as-spun fiber structure in which varying amounts of row nucleation and twisting of lamellar, folded-chain crystal overgrowths occur depending on the spinning conditions. As-spun fiber birefringence was shown to depend primarily on the crystalline orientation. Mechanical properties correlated well with *c*-axis crystalline orientation function and spinline stress.

INTRODUCTION

Since the pioneering work of Carothers and Hill[1] in 1932, it has been realized that the properties of melt-spun, synthetic fibers are highly dependent on the spinning conditions used in their production. This behavior is presumably due to the effect of process variables on the structure of the spun filament. The formation of structure, i.e., crystallinity, orientation, and crystalline morphology, during the melt spinning of a partially crystalline polymer is complicated by the combined influences of rheological factors (stretching of the melt) and nonisothermal effects resulting from the heat transfer from the running filament. Because of these complications and in spite of a rapidly developing industry, early work was largely empirical, and there was little fundamental study of the interaction of rheological behavior and structure formation until the work of Ziabicki and Kedzierska in the late 1950's and early 1960's.[2–6] These authors found that the molecular orientation as measured by birefringence increased with spinline tension, the difference between the take-up and extrusion velocities, and the inverse of the filament diameter.

* Present address: Monsanto, P.O. Box 12830, Pensacola, Florida 32575.

Based upon this early work, Ziabicki[7,8] and others[9-10] have attempted to model the melt spinning process. Only a few of these attempts dealt with the important problem of crystallization and structure development, while most were concerned with the rheological and heat transfer aspects in the upper part of the spinline. These models (for a recent treatment, see, for example, Abbott and White[16]) together with experimental work on melts crystallized while stretching[17-19] or during shearing[20] point to the importance of molecular orientation in the melt on the crystallization kinetics and resulting morphology.

A few experimental studies have attempted to follow the development of structure during the spinning process by measuring such variables as fiber surface temperature, diameter, birefringence,[13,21,22] and obtaining x-ray patterns[23,24] as a function of distance from the spinneret. By far the most complete and significant of these investigations is that of Katayama, Amano, and Nakamura[24] who combined measurements of filament surface temperature, diameter, birefringence, and both wide-angle (WAXS) and small-angle x-ray scattering (SAXS) to study the formation of structure in polyethylene, polypropylene, and polybutene-1. In addition to demonstrating the increase in crystallization kinetics due to molecular orientation during melt spinning, their results showed a morphology consisting of lamellar and interlamellar regions stacked normal to the fiber axis and called attention to the interaction between the heat of crystallization and the rate of heat transfer from the running filament. Katayama and co-workers[14,25] have treated this latter effect in greater detail in more recent publications.

While the studies of Katayama, Amano, Nakamura[24] show the value of experimental measurements along the running threadline in obtaining an understanding of the melt process, it would appear that there is still much to be done. Extension of such studies to a wider range of spinning conditions and to other polymers is needed. Further, until the recent work of Abbott and White[16] from our laboratory, there was almost no information in the open literature relating the structure and spinning variables to the mechanical properties of as-spun fibers. Although the structure and properties of drawn fibers have received much study,[26-32] most of this effort has involved spherulitic fibers and films as starting materials. The effect of the interaction of the melt spinning and drawing processes on the structure and properties developed in the final fiber appears to have received little attention in the open literature. The present investigation represents one installment in a program being carried out in our laboratories to study structure development during melt spinning and its relation to the properties of both as-spun and drawn fibers.

EXPERIMENTAL TECHNIQUES

Special equipment was developed for on-line studies of the development of structure in fibers as a function of spinning conditions. This equipment, which was similar in many respects to that first developed by

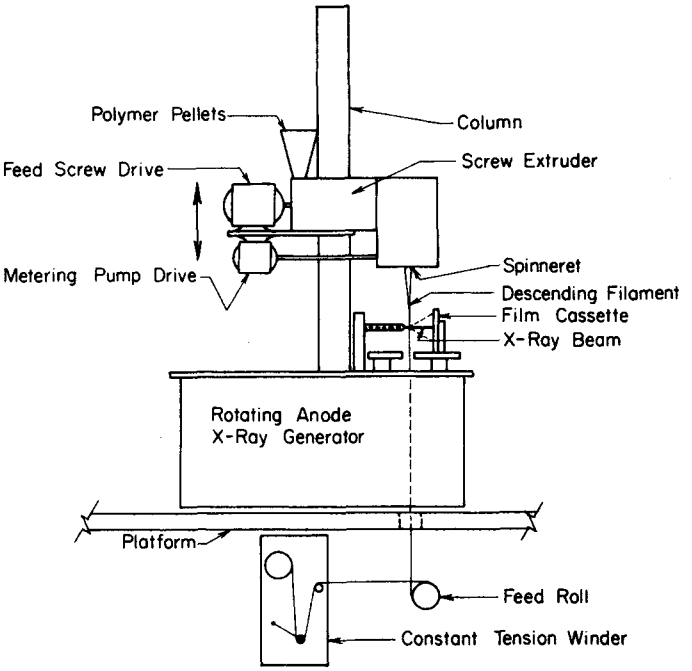

Fig. 1. Schematic of experimental equipment.

Katayama et al.,[24] is shown schematically in Figure 1. The main conponents of the equipment included (1) a screw extruder-metering pump–spinneret combination, manufactured to our specifications by Fourné Associates of West Germany, (2) a 6 KVA Rigaku rotating-anode x-ray generator, (3) a feed roll whose rotational velocity was established by a direct-current motor and speed controller, (4) a Leesona 955 constant-tension winder, and (5) various accessory devices for obtaining wide-angle x-ray diffraction patterns, filament diameter, surface temperature, and tension in the fiber. Monofilaments emanating from the spinneret capillary (0.762 mm in diameter by 3.81 mm long) were passed directly through a collimated CuK_α x-ray beam, through the x-ray generator to the feed roll and constant-tension winder. The entire spinning apparatus could be moved vertically along a large column through a distance of 175 cm. This allowed data to be obtained as a function of distance from the spinneret.

Filament diameter was determined by photographing the running filament, projecting the negative on a screen, measuring the diameter of the projected image, and converting this to actual filament diameter. Surface temperature of the filament was determined using a heated chromel-alumel contact thermocouple and a Leeds and Northrup potentiometer. Fiber tension during spinning was measured using a Rothschild tensiometer with a 0- to 2.5-g measuring range.

The wide-angle x-ray diffraction patterns were recorded on a flat film placed 3 cm from the filament. These patterns were converted to digital format for analysis of crystalline orientation and crystallinity by scanning an entire quadrant of the x-ray pattern with a Tech/Ops scanning microdensitometer.

The orientations in the filaments were characterized quantitatively by computation of the Hermans' orientation factors[33] as generalized to all three crystallographic axes by Stein.[34] This factor is defined as

$$f_x = (3\ \overline{\cos^2\chi} - 1)/2 \tag{1}$$

where $\overline{\cos^2\chi}$ is the average value of the cosine squared of the angle χ between the reference direction in the sample (fiber axis) and the x-crystallographic axis. Assuming rotational symmetry about the fiber axis

$$\overline{\cos^2\chi} = \frac{\int_0^{\pi/2} I_{hkl}(\chi)\ \cos^2\chi\ \sin\chi\ d\chi}{\int_0^{\pi/2} I_{hkl}(\chi)\ \sin\chi\ d\chi} \tag{2}$$

where $I_{hkl}(\chi)$ is the intensity diffracted from the (hkl) planes which are normal to the x-crystallographic direction. The integrals in eq. (2) were evaluated numerically from the intensity distribution in the 200 and 020 reflections to give directly the values of f_a and f_b (a-axis and b-axis orientation) from eq. (1). Since polyethylene is orthorhombic,[34]

$$f_a + f_b + f_c = 0 \tag{3}$$

and f_c could be obtained from the values of f_a and f_b.

X-Ray crystallinity was computed using the Mathews, Peiser, and Richards method[35] corrected for orientation in the sample.

In addition to the on-line studies, several other investigations were carried out on the final spun fibers. These included obtaining small-angle x-ray scattering (SAXS) patterns by both pinhole and Kratky goniometer techniques, determination of pole figures by counter-diffractometer methods, measurement of fiber birefringence, scanning electron microscopy of fiber surfaces, density crystallinity, and tensile properties.

Two batches of polyethylene with similar characteristics (melt indices of 5.0) were used in the study. One batch was Texas Eastman Tenite 3360 and the other was Phillips Marlex EMB-6050. The observed behavior of these two materials during spinning was nearly identical.

RESULTS AND DISCUSSION

Filament Diameter, Velocity, and Temperature Profiles

The filament diameter versus distance from the spinneret is shown for three cases in Figure 2. The sample designations in this and subsequent figures refer to Table I. As the molten polyethylene emerges from the

TABLE I
Spinning Conditions for Linear Polyethylene Samples

Sample designation	Mass flow rate, g/min	Take-up velocity, m/min	Extrusion temperature,[a] °C
PE03	1.93 ± 0.03	50	205
PE01		100	205
PE02		200	205
PE06		400	209
PE07		556	210
PE04		50	180
PE09	0.71 ± 0.02	200	207
PE05	4.00 ± 0.03	100	182

[a] Temperature of polymer measured within extruder.

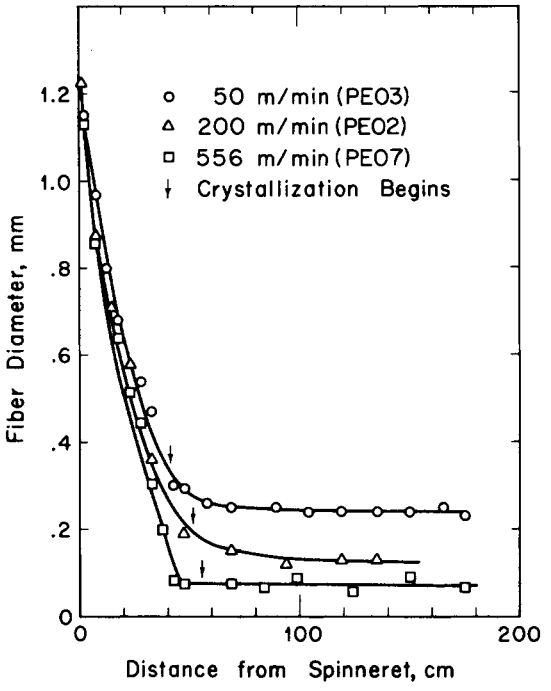

Fig. 2. Filament diameter vs. distance from spinneret.

spinneret, it passes through a die swell region, not shown on the plot, where the filament diameter reaches its maximum size. From that point the diameter decreases as the polymer accelerates, and it reaches a constant value when the material reaches take-up velocity. Several velocity and velocity gradient profiles for the region below the die swell are shown in Figures 3a and 3b. The velocity is low in the die swell region near the spinneret. It increases slowly over a short distance and then rapidly rises to the take-up velocity. In this zone of rapid acceleration the velocity

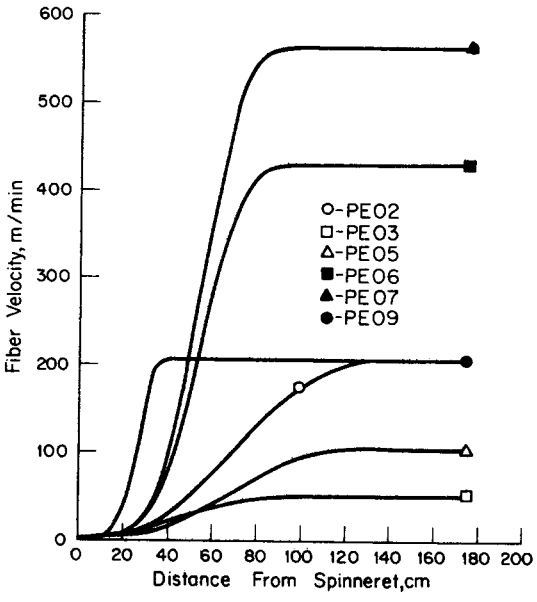

(a)

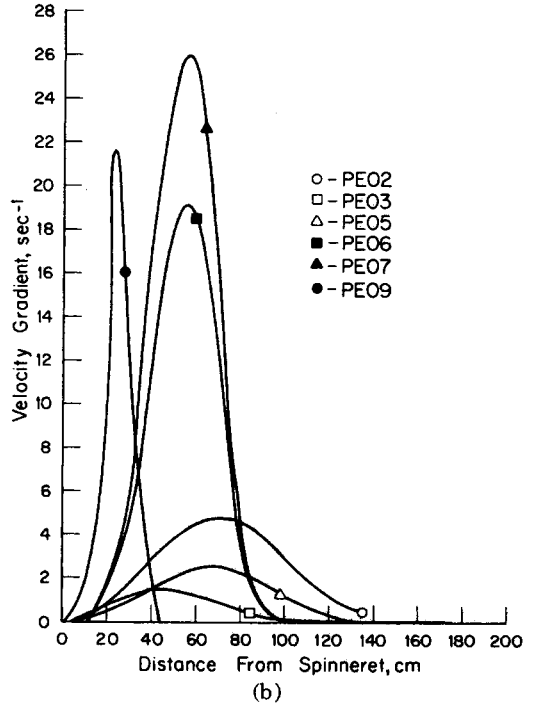

(b)

Fig. 3. Velocity (a) and velocity gradient (b) as a function of distance from spinneret.

gradient rises to a maximum and quickly decreases to zero as the take-up velocity is achieved.

It is clear that increasing the take-up velocity at constant mass flow rate decreases the final fiber diameter and causes the velocity gradient to rise to higher peak values (compare data for samples PE 03, PE 02, PE 06, PE 07). If we assume that to a first approximation the stress is proportional to the velocity gradient (prior to any crystallization), these data demonstrate the increase in stress in the draw-down region with increasing take-up velocity. At a given take-up velocity, decreasing the mass flow rate causes an increase in the rate of draw-down and an increase in spinline stress as illustrated by comparing the results in Figures 3a and 3b for samples PE 05, PE 02, and PE 09.

The peak in the velocity gradient also becomes narrower with decrease in mass flow rate, showing that the draw-down zone becomes shorter. The elongation of a molten filament from the die swell diameter to its final diameter is described by mass, momentum, energy, and constitutive equations as discussed by Ziabicki[2-8] and other workers in the field. Diameter, temperature, and velocity profiles can be approximated by numerical solution of these equations. Specific features of these profiles, such as the shape and location of the maximum velocity gradient, are thus complicated functions of several variables; consequently, simple statements of the effects of individual variables on these specific features are not always possible. This seems to be the case with the maximum velocity gradient calculated for the spinning tests reported here. At constant mass flow rate, an increase in take-up velocity causes the location of the maximum velocity gradient to move further down the spinline initially. With further velocity increases a point is reached where the point of maximum velocity gradient begins to move back toward the spinneret. This behavior is possibly a result of a balance between heat transfer phenomena and the forces acting on the filament. At low speeds, the momentum effects predominate and the maximum velocity gradient moves further down the filament as take-up velocity increases. As higher speeds are reached, cooling of the filament increases dramatically because of smaller fiber diameter and higher velocity. This rapid cooling produces rapid and large changes in rheological properties and the velocity gradient moves back toward the spinneret to maintain the proper momentum balance in the filament.

The increase in elongational velocity gradient (and stress) presumably increases the molecular orientation in the molten polymer, and this in turn enhances crystallization kinetics as will be discussed in more detail in a later section. Crystallization is observed to begin at a point near the peak in the curves of velocity gradient versus distance from the spinneret where the melt stresses are highest. Once crystallization sets in, the velocity gradient rapidly decreases to zero and the diameter becomes essentially constant. The details of this picture are further complicated by the heat transfer occurring from the fiber to its surroundings.

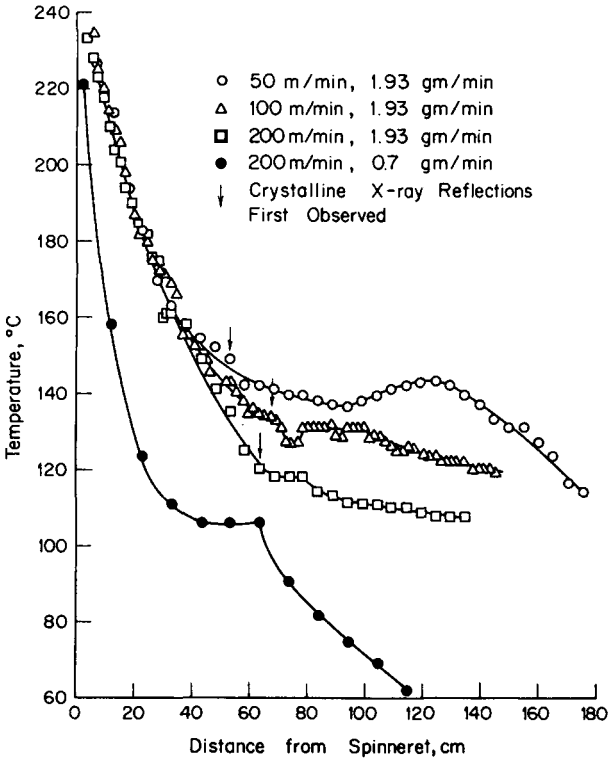

Fig. 4. Fiber surface temperature vs. distance from spinneret.

The fiber surface temperature versus distance from the spinneret is shown in Figure 4. The fiber cools rapidly from the spinneret exit temperature until crystallization begins. The liberation of the enthalpy of crystallization causes a decrease in cooling rate which, in most cases examined, leads to an actual hold, or plateau, in the temperature (in one case, an increase in temperature was observed). After a significant fraction of the crystallization has been completed, the fiber continues to cool, but more slowly as it approaches ambient temperature. It should be noted that the point at which crystalline x-ray peaks were first observed occurred just ahead of the onset of the plateau in the temperature profile as would be expected. The diameter and velocity have almost reached their final values before the temperature plateau begins, and the velocity gradient has decreased significantly from its peak value. These observations are qualitatively consistent with those of Katayama et al.,[24] although a wider range of spinning conditions was investigated in this study.

At constant mass flow rate, the temperature profiles for various take-up velocities were quite similar in the portion of the spinline above the draw-down zone. Upon passing through the draw-down zone, the cooling rate increases with take-up ve ocity because of the increased surface-to-volume ratio caused by the diameter change and also because of higher linear

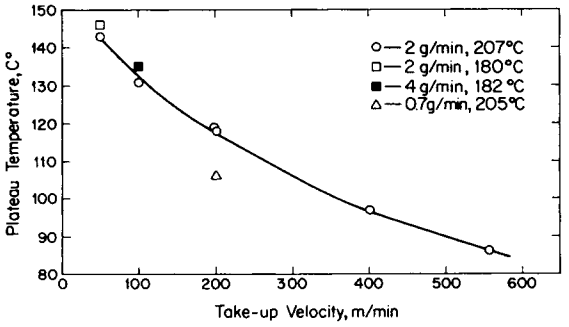

Fig. 5. Temperature of plateau in the temperature profile vs. take-up velocity.

velocity through the cooling medium. A quantitative relationship between heat transfer coefficient and linear velocity has been given by Kase and Matsuo.[10] The increased cooling rate at higher take-up velocities results in a more rapid decrease in fiber temperature with distance from the spinneret and in lower crystallization plateau temperatures. An increase in cooling rate is also obtained by decreasing the mass flow rate at constant take-up velocity. The plateau temperature is plotted versus take-up velocity for several runs in Figure 5.

Crystallization temperatures for the Tenite polymer crystallized under quiescent conditions in a differential scanning calorimeter (DSC) are shown in Table II. The crystallization temperatures for samples cooled at rather modest cooling rates in the DSC are much lower than the plateau temperatures of several of the melt spinning runs. The cooling rates during melt spinning at temperatures near the plateau lie in the range of 50°C/sec to 2100°C/sec for take-up velocities between 50 and 556 in./min at a mass flow rate of 1.93 g/min. The relatively high crystallization temperatures associated with rapid cooling conditions existing during melt spinning indicate that molecular orientation resulting from the elongational flow and drawn-down forces in the filament greatly increase crystallization rate. Although this idea has been proposed by previous investigators,[16,24] it is clear from the present data that in the case of linear polyethylene, only relatively modest spinning conditions are required to provide a sizable effect. It is also interesting that at low take-up velocities (ca. 50 m/min), crystallization proceeds at temperatures near or slightly above the melting point of the polymer crystallized under quiescent conditions. (Although the thermocouple was calibrated under static conditions, no truly accurate method has yet been found for calibration on the running threadline. The measured temperatures may therefore be slightly too high due to the friction of the thermocouple in contact with the moving filament. Efforts were made to reduce this source of error, and we believe that the reported temperatures are accurate within 2° to 3°C.)

At any take-up velocity and mass flow rate, the temperature at which crystallization begins is the result of a balance between the supercooling

TABLE II
Crystallization of Tenite Linear Polyethylene in DSC

DSC cooling Rate,[a] °C/min	Start of crystallization,[b] °C	Peak of exotherm,[b] °C
5	119	116
10	118	114
20	115	111

[a] All samples held 15 min at 205°C prior to cooling.
[b] Average of two runs at each cooling rate.

effect provided by the high cooling rate and the increased crystallization rate caused by the molecular orientation in the filament. Since the crystallization temperature decreases with increasing take-up velocity in the range above 50 m/min, it would appear that in this range the increased cooling rates overide any increase in crystallization kinetics resulting from increased molecular orientation. The reverse must of course be true in some very low take-up velocity range. It is suggested that these facts are caused by the tendency for the effect of spinline deformation rate (or stress) on the crystallization kinetics to saturate at relatively low levels in the case of linear polyethylene while the cooling rate continues to increase rapidly with increasing take-up velocity. Further support for this contention is presented in the next section.

Wide-Angle X-Ray Diffraction—Development of Crystallinity

Plots of per cent crystallinity versus distance from the spinneret derived from the x-ray patterns taken along the spinline during operation are presented in Figure 6. Figure 6a is an example showing the x-ray patterns and typical data scatter. Figure 6b shows a comparison between the results for several runs. It should be realized that the crystalline orientation developed, and hence the appearance of the x-ray patterns, varies considerably from run to run. This will be discussed in detail below after discussion of the crystallization rates.

Crystallization begins at a point in the filament near the maximum in the velocity gradient and continues as the filament moves to the take-up bobbin. A large fraction of the final crystallinity, of the order of 60%, is developed prior to the end of the temperature plateau, but some increase in crystallinity continues further down the spinline. This behavior agrees with that expected for a material that remains above its glass transition temperature throughout the entire spinning process. Except for a reversal at the highest take-up speed, the polymer starts crystallizing slightly further down the spinline and progresses to a lower ultimate crystallinity (see Table III) as spinning speed increases. This latter behavior was also observed by Abbott and White[16] and was attributed to the increased cooling rate at the higher take-up velocity as previously mentioned (compare samples PE 03, PE 02, PE 06, and PE 07).

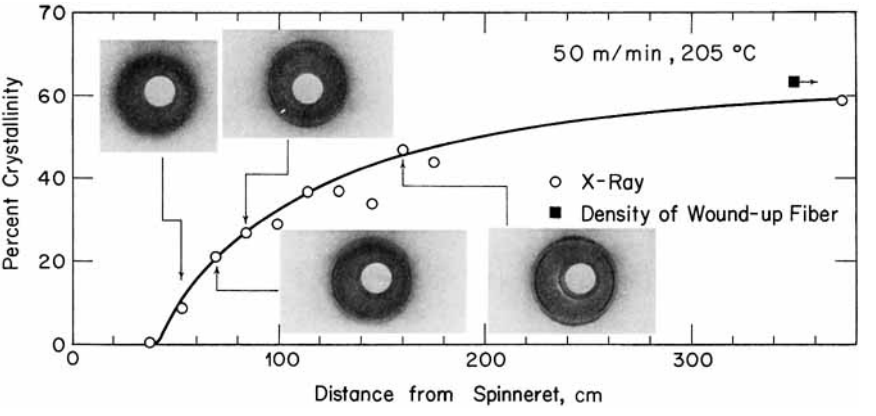

(a)

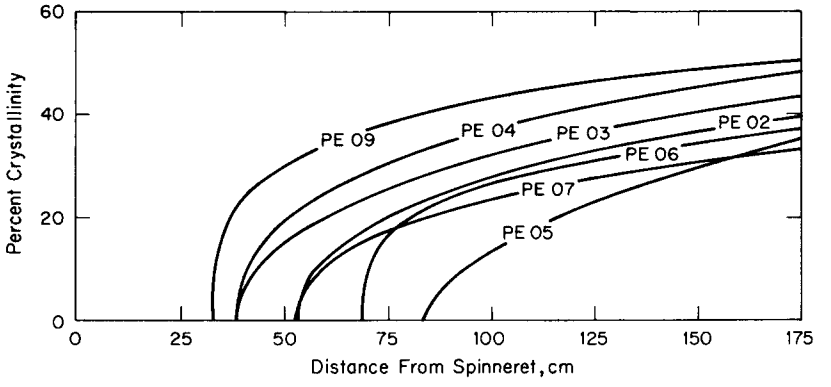

(b)

Fig. 6. Crystallinity vs. distance from spinneret: (a) typical results; (b) comparison of results for several runs.

One effect of mass flow rate clearly evident in Figure 6b is to move the point at which crystallization begins further from the spinneret with increasing flow rate (compare PE 05, PE 02, and PE 09). Decreasing the mass flow rate at a given take-up velocity increases the cooling rate (Fig. 4), increases the maximum velocity gradient and stress, and thereby would be expected to increase crystallization rates.

Conditions that increase the filament stress cause the curves in Figure 6b to rise abruptly as crystallization begins (samples PE 06 and PE 09), while low spinline stresses lead to a more gradual rise in crystallinity with distance (PE 03 and PE 05).

Figure 7 shows the per cent crystallinity for a volume element in the filament versus a time scale calculated from the velocity profiles. Figure 7a shows the effect of increasing take-up velocity at constant mass flow rate and extrusion temperature. The time plotted is measured from the point of extrusion. Figure 7b shows the effect of changing the mass

TABLE III
Crystallization Half-Times During Melt Spinning

Mass flow rate, g/min	Take-up velocity, m/min	Extrusion temp.,[a] °C	Spinning stress, (dynes/cm²) × 10^{-8}	Crystallization temp.,[b] °C	Ultimate crystallinity,[c] %	Spinning half-time,[d] sec	Isothermal half-time,[e] sec
1.93 ± 0.03	50	205	1.0	143	63.4	0.65	—
	100	205	2.8	131	62.3	0.61	2.3×10^7 (36), 398 (38)
	200	205	5.5	118	61.7	0.51	306 (36)
	400	209	10.0	97	57.2	0.17	2.2×10^5 (36)
	556	210	17.1	86	57.7	0.08	3.8×10^8 (36)
	50	180	2.1	146	66.0	0.46	—
0.71 ± 0.02	200	207	12.1	106	59.4	0.44	3.5×10^3 (36)
4.00 ± 0.03	100	182	1.8	136	64.0	0.90	$>10^{12}$ (36), 885 (38)

[a] Temperature of polymer measured within extruder.
[b] Temperature of plateau in surface temperature vs. distance from spinneret curve.
[c] From density of wound-up fiber.
[d] Time to reach 50% of the ultimate crystallinity starting from the point at which the surface temperature is 150°C.
[e] Crystallization half-times for quiescent, isothermal conditions. Numbers in parentheses refer to list of references.

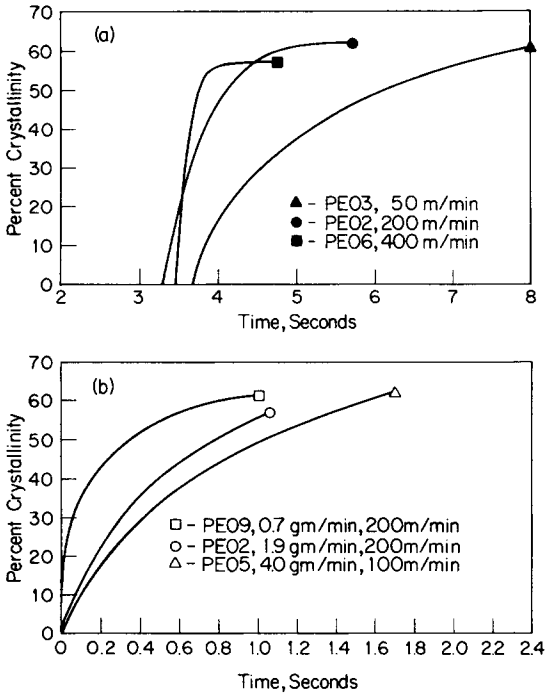

Fig. 7. (a) Crystallinity vs. time after leaving spinneret showing effect of increasing take-up velocity at constant mass flow rate, (b) crystallinity vs. time from start of crystallization showing effect of changing the mass flow rate.

flow rate. Because changing the mass flow rate has a marked effect upon the time the polymer spends in the molten zone, it is more meaningful for intercomparison to measure crystallization time from the start of crystallization rather than from extrusion in this case. The effect of changing either the take-up velocity or mass flow rate may be interpreted in terms of the effect these changes have on the stress and the cooling rate of the filament. At constant mass flow rate, an increase in take-up velocity will result in an increase in both stress and cooling rate in the filament leading to increased crystallization rates (Fig. 7a). At a fixed spinning speed, an increase in mass flow rate will cause an increase in filament cross-sectional area and a slight change in tension, with the net result being a decrease in stress. The larger diameter also results in a decrease in cooling rate. These factors thus lead to a decrease in crystallization rates.

Referring again to Figure 7a, the rate change on increasing the take-up velocity from 50 to 200 m/min is rather large compared with the change from 200 to 400 m/min. We interpret this to mean that the effect of orientation in the melt on the crystallization rate is approaching a limiting value in the range of spinning conditions investigated.

The time required to reach one half the final crystallinity measured from a point at which the fiber temperature was 150°C is given together with the spinline stress (based on final diameter) in Table III. The choice of 150°C as the temperature from which to measure crystallization times was arbitrary but based on the idea that above this temperature the filament would not be expected to have any tendency toward crystallization even with molecular orientation. Since more than half the crystallization occurred at the plateau temperature, this temperature is also given in Table II. For comparison, the time to reach one half the ultimate crystallinity under quiescent isothermal conditions at a temperature corresponding to the plateau temperature is also given. The first values presented were obtained by fitting the data given by Mandelkern[36] to the equation given by Takayanagi and Kusumoto[37] for the temperature dependence of the crystallization rate constant and then computing from this equation the values of crystallization half-time at the appropriate temperatures. Although differences in polymers and small errors in temperature can make large changes in the comparisons, it is clear that a conservative estimate of at least a several hundredfold increase in crystallization rate occurs during melt spinning as compared to quiescent conditions. Increases in crystallization rate of about the same order observed here have been observed by Haas and Maxwell[20] in linear polyethylene crystallized under shear stress.

Wide-Angle X-Ray Diffraction—Development of Orientation

Crystalline orientation was observed in all samples investigated. The orientation in gravitationally spun filaments (no take-up stress except the filaments' own weight) was small but present for conditions where the spinline had appreciable length. At a take-up velocity of 50 m/min and above the 020 reflection was concentrated near the equator, thus indicating a tendency for the *b*-axes of the orthorhombic polyethylene unit cells to lie perpendicular to the fiber axis. The intensity distribution around the 200 reflection varied markedly with take-up velocity. It exhibited a maximum on the meridian at low take-up velocities, but this changes to a maximum on the equator at higher take-up velocities. This effect may be observed clearly and quantitatively in the pole figures presented in Figure 8. These results were obtained using a short, parallel bundle of fibers and a counter diffractometer technique.

The values of the orientation functions f_a, f_b, and f_c computed from the diffractometer data are shown plotted as a function of take-up velocity in Figure 9. According to eq. (1), the values of the orientation functions should be zero for a random sample. If an axis is parallel to the fiber axis, the orientation for that axis is 1.0; and if an axis is perpendicular to the fiber axis, the respective orientation function is -0.5. With increasing take-up velocity, f_c increases, indicating a tendency for the *c*-axes to align with the fiber axis. The value of f_b rapidly decreases to values near -0.4, indicating that the *b*-axes are nearly perpendicular to the fiber axis. The behavior of f_a, first increasing and then decreasing, is more complex and

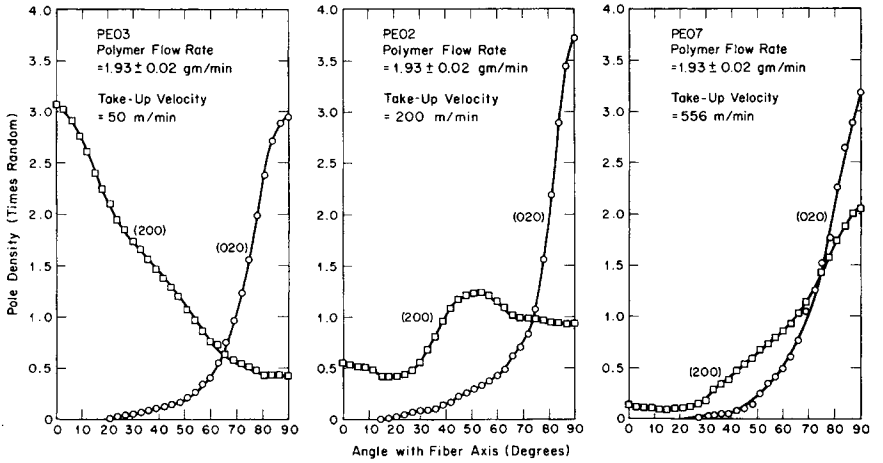

Fig. 8. Pole density distributions for the (200) and (020) reflections at take-up velocities of (a) 50 m/min, (b) 200 m/min, and (c) 556 m/min.

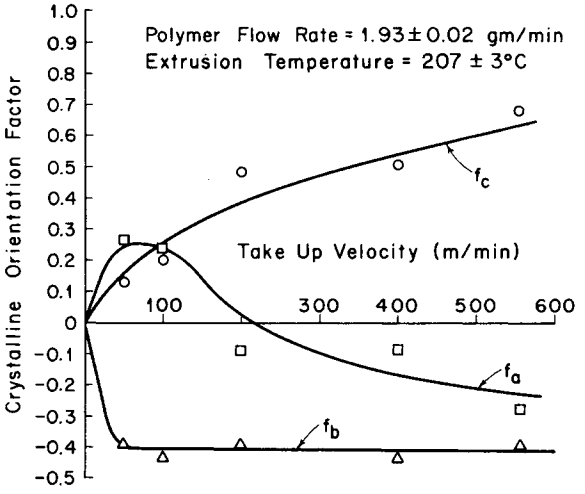

Fig. 9. Crystalline orientation functions vs. take-up velocity.

will be considered in detail later. Similar trends in the variation of the orientation functions with take-up velocity have been observed by previous investigators in our laboratory[16] at mass flow rates both higher (5 g/min) and lower (0.5 g/min) than those used in the present investigation. As mass flow rate decreases the take-up velocity at which f_c rises rapidly and f_a goes negative also decreases.

Figure 10 shows the variation of f_a, f_b, and f_c as a function of position along the spinline for three different take-up velocities. These values were computed from the microdensitometer scans of the WAXS patterns made during spinning. The trends observed in the three examples shown are typical of the observed behavior. At both low and high take-up velocities

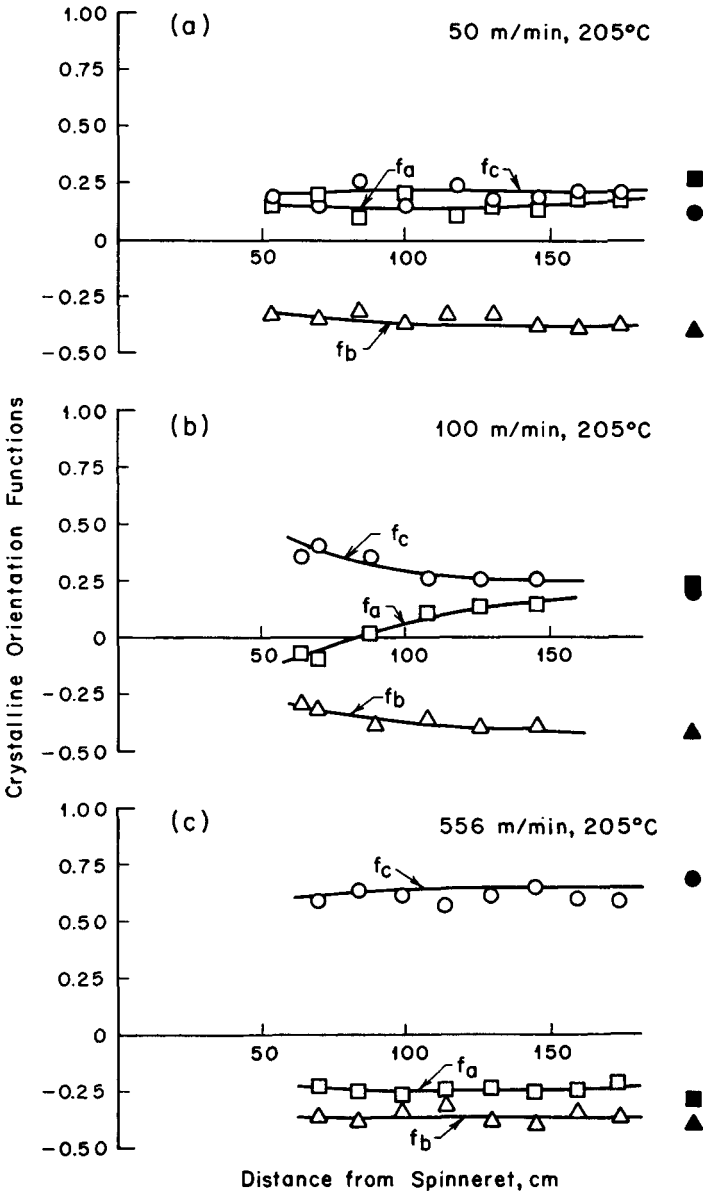

Fig. 10. Variation of crystalline orientation functions along spinline for take-up velocities of (a) 50 m/min, (b) 100 m/min, and (c) 556 m/min.

(50 m/min and 556 m/min), the orientation is very similar to that observed in the final fiber from the point at which the crystalline reflections could first be observed onward. In the intermediate take-up velocity range (100–200 m/min), the *a*- and *c*-axis orientation functions were observed to change along the spinning way as shown in Figure 10b. The *a*-axis orientation

function increases from a negative to a positive value, while the *c*-axis orientation function decreases. During the early stages of crystallization, the observed patterns are similar to those developed at higher take-up velocities (and therefore high stress). Further down the spinline, the patterns change toward those observed for lower take-up velocities. A similar change in *c*-axis orientation along the spinning way was observed by Katayama et al.,[24] but their spinning conditions were evidently not sufficiently diversified to observe the other extreme conditions shown in Figure 10. They attributed the decrease in *c*-axis orientation to a sudden tilting of the polyethylene chains within lamellar crystals. Our interpretation differs from this; it will be presented in the discussion of fiber morphology.

Small-Angle X-Ray Scattering

The SAXS results are presented in Figure 11 and Table IV. The patterns in Figure 11 show that there is a strong intensity maximum on the meridian for a take-up velocity as low as 50 m/min. It should be noted, however, that the intensity spreads around the incident beam at low take-up velocities and that this effect disappears as take-up velocity increases. If we assume the usual interpretation that the merdional maxima are caused by alternating lamellar crystalline and amorphous (or disordered regions) along the fiber axis direction, the intensity spread can be associated with a spread in the orientations of the lamellar crystals. This is also

TABLE IV
Long Periods of Spun Fibers

Mass flow rate, g/min	Take-up velocity, m/min	Long period, Å
1.93 ± 0.03	50	247
	100	239
	200	226
	400	227
	556	229
	50	248
0.71 ± 0.02	200	220
4.00 ± 0.03	100	248

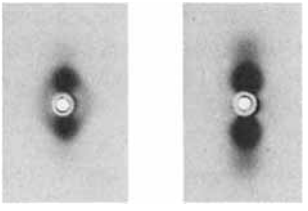

Fig. 11. Pinhole SAXS patterns for (a) low take-up velocity (50 m/min, PE 03) and (b) relatively high take-up velocity (400 m/min, PE 06).

consistent with the increase in *c*-axis orientation parallel to the fiber axis with increasing take-up velocity as shown in Figure 9.

A weak second-order peak was observed on the meridian in the original patterns, and, if highly overexposed, a third order maximum could be observed on samples spun at the highest take-up velocities. This is further evidence for a fairly regular stacking of lamellar and interlamellar regions parallel to the fiber axis. Patterns for as-spun fibers similar to our high take-up velocity cases showing second- and third-order maxima have previously been published by Statton,[39] although the spinning conditions were not given.

Quantitative SAXS results were obtained using a Kratky goniometer equipped with a proportional counter. The values of long-period spacing shown in Table IV were computed by applying Bragg's law to the centroids of the first-order maxima in the scattering curves. Although the changes are not large, there seems to be a trend toward smaller long periods with increasing take-up velocity and decreasing mass flow rate. Recalling that the temperature at which much of the crystallization occurred decreased and the stress in the draw-down region increased with increasing take-up velocity and decreasing mass flow rate, the observed trend seems reasonable.

The values of the long-period spacings in our spun fibers are much smaller at similar crystallization temperatures than those observed by Kavesh and Schultz[40] for quiescent melts, and our values do not vary as much with crystallization temperature. Our results are consistent with Statton's values for melt-spun fibers, however.[39] The differences between the long-period spacings for quiescent melts and melt-spun fibers is undoubtedly associated with the more rapid crystallization kinetics caused by molecular orientation.

Scanning Electron Microscopy

The surfaces of the spun fibers were examined in a scanning electron microscope. A lamellar texture perpendicular to the fiber axis was observed. Since the resolution of this instrument is insufficient to clearly resolve lamellae of approximately 200-Å dimensions, the observed texture probably consisted of "bundles" of lamellar crystals. The appearance of the texture varied somewhat with spinning conditions, as shown in Figures 12a and 12b. With increasing take-up velocity, the surface texture became finer and somewhat more uniform.

Lamellae perpendicular to the fiber axis in melt-spun polyethylene have also been observed by Fung and Carr[41] using transmission electron microscopy (replica technique).

Birefringence, Tensile Properties, and Role of Spinline Stress

At a given mass flow rate and polymer extrusion temperature, the spinline stress increases rapidly with take-up velocity. For example, at a mass flow rate of 1.93 g/min and an extrusion temperature of 205°C, the

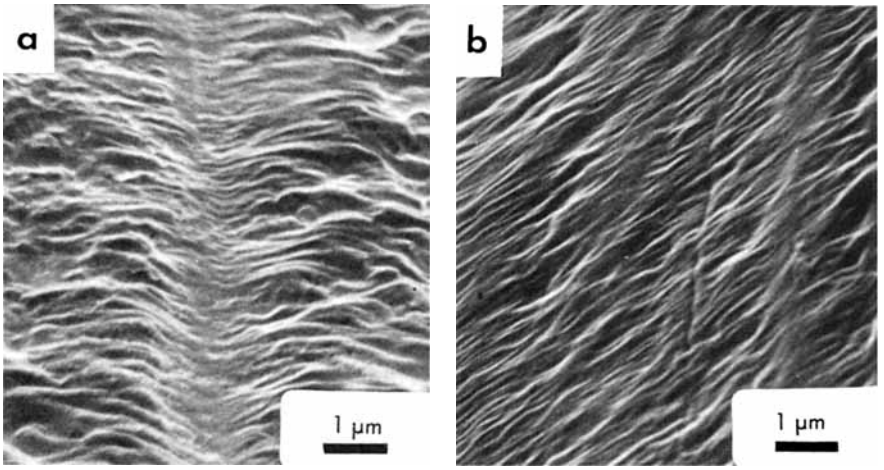

Fig. 12. Scanning electron micrographs of surface texture of polyethylene fibers spun with take-up velocities of (a) 50 m/min and (b) 556 m/min. Fiber axis is vertical. The apparent tilt of the lamellar texture relative to the fiber axis in (b) is an artifact caused by the direction of observation of the curved surface of the fiber. The lamellae are actually perpendicular to the fiber axis.

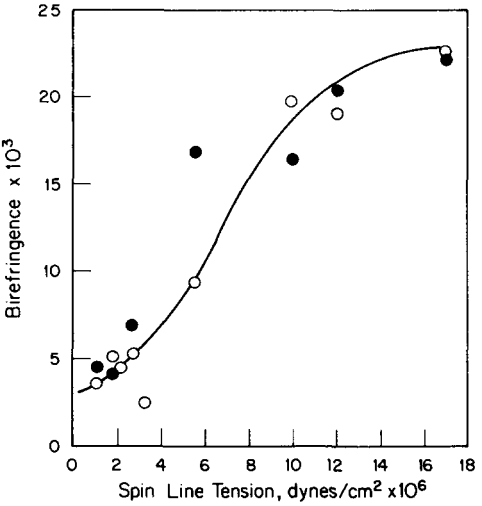

Fig. 13. Birefringence of fiber vs. stress during spinning.

spinline stress increases by a factor of about 17 with an increase in take-up velocity from 50 to 556 m/min (see Table III). Spinline stress also increases with decreasing mass flow rate or decreasing extrusion temperature. Thus, the important effect of such variables as take-up velocity and mass flow rate on the orientation developed in the fiber can be traced largely to the effect of these variables on the spinline stress.

Figure 13 shows experimental values of as-spun fiber birefringence plotted as a function of spinline stress. As the stress increases, the *c*-axis orientation, and hence the birefringence, increases steadily. This figure

also shows values of crystalline birefringence calculated from the following equation[26,42]:

$$x_c\Delta_c = x_c \frac{2}{9} \pi \frac{(\eta^2 + 2)^2}{\eta} (\alpha_\parallel - \alpha_\perp) f_c \tag{4}$$

using our orientation functions and density crystallinity values together with the values of the other parameters given by Stein and Norris.[26] In eq. (4), η is the average refractive index and $\alpha_\parallel$ and $\alpha_\perp$ are the average polarizabilities per unit volume of the crystal parallel to and perpendicular to the c-axis. Within the experimental accuracy of our birefringence, orientation function, and crystallinity results, it would appear that the total birefringence of these as-spun fibers is given by the crystalline contribution (a small negative contribution by the amorphous fraction may be indicated over part of the range). This result is perhaps not surprising in view of the high crystallinities of these linear polyethylene filaments and the likelihood that the "amorphous" portions probably consist of loose chain folds between the lamellar crystals together with various structural defects.

The tensile strength, elongation to break, and Young's modulus of as-spun linear polyethylene fibers are shown in Figure 14 plotted versus the crystalline orientation function f_c. A strong correlation is observed between the c-axis orientation and each of the measured properties. Since the crystallinity (density) of the fibers only varies from 57% to 66% (see Table III), the effect of such variation *per se* on the properties should be small. The large differences in properties, therefore, appear to be a consequence of the molecular orientation and/or changes in morphology with spinning conditions.

Investigators studying drawn fibers[30,31,43] prepared from low-orientation starting materials have argued that the amorphous orientation, particularly the number of tie molecules, is of overriding importance in determining the mechanical properties. As spinline stress increases, we might expect the greater molecular orientation developed in the molten zone to create larger numbers of tie molecules in the spun fiber and, thereby, lead to the observed increases in modulus and tensile strength. In as-spun polyethylene fiber, our data indicate that the amorphous contribution to birefringence is small over the entire range of spinning conditions investigated. Hence, this parameter is clearly not a useful measure of the number of tie molecules or other factors which control the mechanical properties in such samples.

The strong correlation of the properties with c-axis crystalline orientation function may arise from two factors. In the first case the factors which lead to increased c-axis orientation may also lead to increased numbers of tie molecules as already mentioned. The mechanical properties correlate at least as well with spinline stress as they do with the c-axis crystalline orientation function. This fact may be quite useful from a technical point of view since spinline stress is relatively easy to measure.

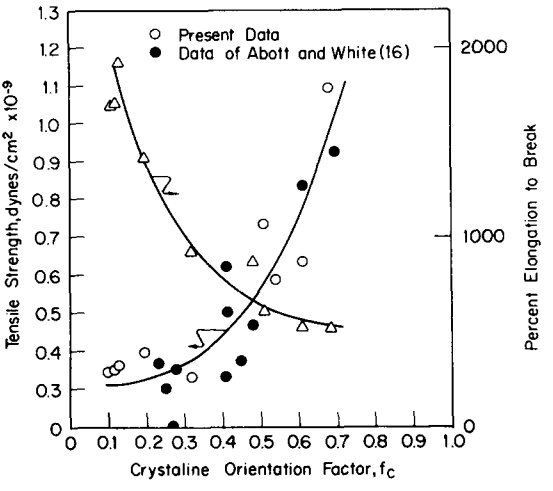

Fig. 14. Mechanical properties of fibers vs. c-axis crystalline orientation function. (a) Tensile strength and elongation to break; (b) Young's modulus.

The second factor relates to the ease of deformation (both elastic and plastic) of the crystals themselves as a function of orientation and the details of their interconnection by tie molecules.

Morphologic Model for Melt-Spun Linear Polyethylene Fiber

Our data, together with that of previous investigators, allow a rather detailed interpretation of the morphology of the spun fibers and how this varies with spinning conditions. The evidence cited for strain-induced nucleation, the two-point SAXS patterns, and the scanning electron microscopy suggest a "row nucleated" structure. These data, taken together with the WAXS data, suggest the morphologic development presented schematically in Figure 15. The model is based upon the interpretation first given by Keller and co-workers[18,19] to results from samples crystallized

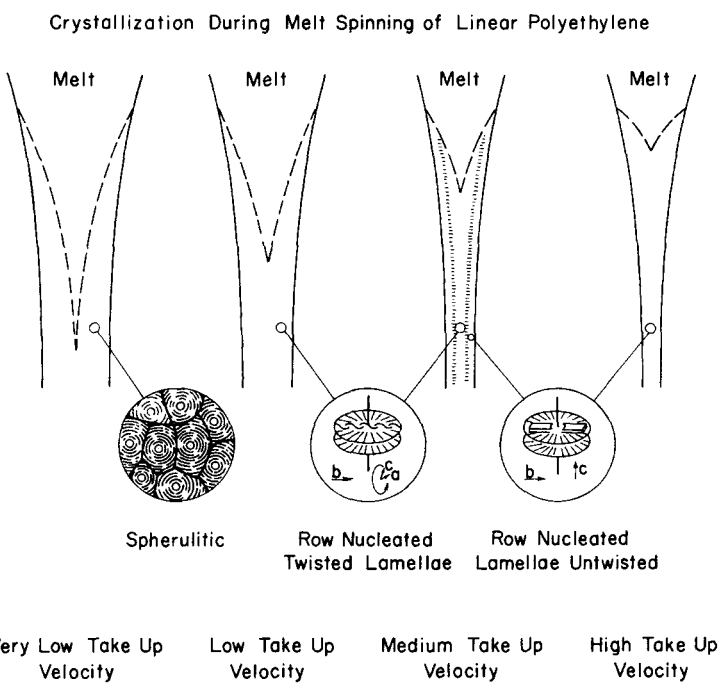

Fig. 15. Morphologic model of structures developed in as-spun linear polyethylene.

during stretching of the melt. Ribbon-like, lamellar polyethylene crystals are nucleated by, and grow epitaxially on, fibril nuclei generated by the elongational straining and orientation of the melt. The lamellar crystals may twist as they grow outward from the fibril nucleus if the stress is low, just as they apparently do during the growth of polyethylene spherulites in quiescent melts.[44] During crystallization at higher levels of stress, the ribbon-like crystals do not exhibit as much twist. A model similar to that discussed here has been developed by Clark and Garber[45] to explain the morphology of blown film and injection-molded poly(oxymethylene). These authors also suggested that such an approach might be applicable to fiber spinning.

In applying this model to our data for melt-spun fibers, it should be kept in mind that the direction of growth of the polyethylene crystals is along the *b*-axis of the polyethylene unit cell. Assuming that the *c*-axis, the chain direction, is perpendicular to the flat face of the ribbon-like crystals while the *a*-axis lies in the plane of the ribbon, regular twisting of the lamellae causes a rotation of the *a*- and *c*-axes about the growth direction of the lamellar crystal. Thus, if we calculate Hermans' orientation functions for the extreme, idealized case corresponding to all lamellar crystals growing perpendicular to the fiber axis, but regularly twisting, we obtain $f_a = f_c = +0.25$ and $f_b = -0.5$. For the case that the lamellae do not twist, $f_a = f_b = -0.5$ and $f_c = 1.0$. Comparing these values to the experimental

results shown in Figure 9, we observe that the peak in the value of f_a corresponds to regular twisting of the lamellae, while the decreasing values at higher take-up velocities may be interpreted as a tendency for the lamellae to be less twisted, on the average. The spreading of the SAXS maximum about the incident beam occurs for samples with considerable lamellar twisting.

The orientation data taken as a function of position along the spinline (Fig. 8) may be interpreted as indicating that at low take-up velocity (50 m/min), ribbon-like lamellar crystals twist as they grow outward from the fibril nuclei from the beginning of crystallization as well as on the average, throughout the final filament. Similarly, at high take-up velocities (556 m/min), the lamellae are relatively untwisted throughout the crystallization process. In the intermediate range of take-up velocities ($\approx$100–200 m/min), crystallization begins near the outer surface of the filament owing to the lower temperature at this point resulting from the radial heat transfer from the filament. This slightly lower temperature results in higher viscosity and stress in this region, which then leads at these take-up velocities to growth of relatively untwisted lamellar crystals in this "skin" layer. Once this layer is formed, it supports most of the load; crystallization continues throughout the inner portion of the filament at lower stress and therefore greater helicoidal twisting of the lamellae. The net effect is an overall decrease in c-axis orientation function with distance down the spinline. Further evidence of a "skin effect" in melt-spun filaments is contained in the birefringence measurements of Katayama et al.,[24] Fung and Carr,[41] and in the scanning electron microscopy studies of Billica et al.[46]

For linear polyethylene, the transition from spherulitic crystallization to a row-nucleated morphology apparently occurs at very low levels of spinline stress. We interpret the data shown in Figure 9 to indicate that at a mass flow rate of 1.93 g/min, this transition occurs in the range of take-up velocities between 0 and 50 m/min. This is also consistent with the trends observed in the crystallization kinetics, including the large increases in crystallization rates at relatively low levels of spinline stress and the tendency for saturation of crystallization rates at higher stress levels.

The model proposed by Katayama et al.[24] involving row-nucleated lamellar crystals stacked normal to the fiber axis with the chains tilted at an angle within each crystal is a possible interpretation consistent with the data from fibers spun under conditions which produce textures similar to our intermediate take-up velocity range. This model has several shortcomings, however, when considered in the light of all the available experimental results. For example, the reason given for the "sudden tilting" of the c-axis direction away from the fiber axis is that stress on crystals formed previously causes the chain tilting. This would imply that fiber spun at higher stress levels should exhibit greater chain tilting rather than less, in contradiction to the observed behavior. The model of Katayama et al., thus, does not provide an integrated picture of how the crystalline texture

changes from the spherulitic condition which exists in gravitationally spun fiber to the texture observed in the filaments spun under high spinline stresses.

In recent years, a number of industrial laboratories have developed partially crystalline fibers and films having a high degree of almost rubber-like elasticity. A mechanism for such behavior has been discussed by Clark[47] and by Sprague.[48] These investigators envision such materials to consist of a row structure in which the lamellae are bound together at various points by short tie molecules. When a force is applied to such a material perpendicular to the lamellae, spaces open between lamellae except at tie points. The lamellae themselves deform (bend) elastically and can recover their original form when the force is removed. The type of model envisioned for these so-called "hard" elastic fibers and films would appear to result according to our data from spinning under conditions of high spinline stress where the row structure is well developed. Although none of our as-spun polyethylene fibers exhibited this remarkable elasticity, it is not clear whether this is due to the need for still higher spinning tension, some annealing treatment, or some inherent difference between linear polyethylene and those polymers such as polypropylene and poly(oxymethylene) which have been prepared in this highly elastic form.

SUMMARY AND CONCLUSIONS

An experimental study of the melt spinning of linear polyethylene has been conducted using both measurements carried out on final as-spun fiber and measurements carried out on the filament during the spinning process. The on-line studies included measurement of fiber surface temperature, diameter, spinline tension, crystalline orientation, and crystallinity as a function of distance from the spinneret. The latter two quantities were obtained from x-ray diffraction patterns made on the running monofilament. Investigation techniques used for the final fiber included both wide-angle and small-angle x-ray diffraction, density crystallinity, birefringence, and scanning electron microscopy of the fiber surface texture.

These investigations have allowed us to propose a detailed morphologic model for the structure of the final as-spun polyethylene fiber and to relate the morphology to the processing conditions. The evidence indicates that molecular orientation in the melt results in the formation of fibril nuclei and row nucleation at relatively low spinline stress or take-up velocity. Thus, as take-up velocity increases at a constant polymer mass flow rate, there is a rapid transition from the spherulitic structure occurring in quiescent melts and gravitationally spun fibers to a row-nucleated structure. The row structure formed under these low stress conditions has lamellae growing out from the fibril nuclei and perpendicular to the fiber axis. These lamellae twist in a fashion similar to the twisting which occurs in the radial direction for lamellar crystals growing from the center of spherulites. At higher take-up velocities and spinline stresses, the lamellar crystals

making up the row structure do not twist as much. It was concluded that a skin-core effect existed in at least some melt-spun polyethylene fibers, and a mechanism for its formation was suggested.

Strain-induced fibril nucleation causes crystallization to occur at temperatures far above those at which crystallization occurs for a quiescent melt cooled at similar rates. Further increases in take-up velocity beyond the point at which significant row nucleation first occurs causes the cooling rate to increase rapidly enough to suppress the crystallization temperature, in spite of any additional increase in crystallization rates caused by increased spinline stresses. Crystallization under these conditions results in smaller interlamellar spacings (long periods).

It was concluded from an analysis of the birefringence measurements that the contribution from the amorphous portion of the sample was so small as to be essentially negligible.

The mechanical properties of the fiber correlated well with *c*-axis crystalline orientation function and with the spinline stress. Although plausible explanations for this behavior were given, a detailed quantitative treatment remains to be developed.

The authors thank Professors J. L. White and E. S. Clark and several students in the Department of Chemical and Metallurgical Engineering who contributed considerably to this research through both discussions and deeds. They also express their gratitude to the National Science Foundation for support of the project under Grant No. GK 18897 and to the Monsanto Chemical Company for partial support of one of us (J.R.D.).

References

1. W. H. Carothers and J. W. Hill, *J. Amer. Chem. Soc.*, **54**, 1579 (1932).
2. A. Ziabicki and K. Kedzierska, *J. Appl. Polym. Sci.*, **2**, 14 (1959).
3. A. Ziabicki and K. Kedzierska, *Kolloid Z.*, **171**, 52 (1960).
4. A. Ziabicki and K. Kedzierska, *Kolloid Z.*, **175**, 14 (1961).
5. A. Ziabicki and K. Kedzierska, *J. Appl. Polym. Sci.*, **6**, 111 (1962).
6. A. Ziabicki and K. Kedzierska, *J. Appl. Polym. Sci.*, **6**, 361 (1962).
7. A. Ziabicki, *Appl. Polym. Symp.*, **6**, 1 (1967).
8. A. Ziabicki, unpublished results, 1971.
9. J. L. White, *J. Appl. Polym. Sci.*, **8**, 2339 (1964).
10. S. Kase and T. Matsuo, *J. Polym. Sci.*, **A3**, 2541 (1965).
11. M. E. Morrison, *A.I.Ch.E. J.*, **16**, 57 (1970).
12. C. D. Han, *Rheol. Acta*, **9**, 355 (1970).
13. D. Acierno, J. N. Dalton, J. M. Rodriguez, and J. L. White, *J. Appl. Polym. Sci.*, **15**, 2395 (1971).
14. K. Nakamura, T. Watanabe, K. Katayama, and T. Amano, *J. Appl. Polym. Sci.*, **16**, 1077 (1972).
15. J. A. Spearot and A. B. Metzner, *Trans. Soc. Rheol.*, **16**, 495 (1972).
16. L. E. Abbott and J. L. White, *U.S.-Japan Seminar on Polymer Processing and Rheology*, D. C. Bogue, M. Yamamoto, and J. L. White, Eds. *Appl. Polym. Symp.*, **20**, 247 (1973).
17. A. Keller, *J. Polym. Sci.*, **15**, 31 (1955).
18. A. Keller and M. J. Machin, *J. Macromol. Sci., (Phys.)*, **B1**(1), 41 (1967).
19. M. J. Hill and A. Keller, *J. Macromol. Sci.*, **133**, 153 (1969).
20. T. W. Haas and B. Maxwell, *Polym. Eng. Sci.*, **9**, 225 (1969).

21. A. B. Thompson, in *Fibre Structure*, J. W. S. Hearle and R. H. Peters, Eds., Textile Inst., Butterworths, Manchester, 1963.
22. T. Ishibashi, K. Aoki, and T. Ishii, *J. Appl. Polym. Sci.*, **14**, 1597 (1970).
23. F. P. Chappell, M. F. Culpin, R. G. Gosden, and T. G. Tranter, *J. Appl. Chem.*, **14**, 12 (1964).
24. K. Katayama, T. Amano, and K. Nakamura, *Kolloid-Z.-Z. Polym.*, **226**, 125 (1968).
25. K. Nakamura, T. Watanabe, T. Amano, and K. Katayama, submitted for publication, 1973.
26. R. S. Stein and F. N. Norris, *J. Polym. Sci.*, **21**, 381 (1956).
27. W. C. Sheehan and T. B. Cole, *J. Appl. Polym. Sci.*, **8**, 2359 (1964).
28. R. J. Samuels, *J. Polym. Sci.*, **C20**, 253 (1967).
29. R. J. Samuels, *J. Polym. Sci.*, **6**, 2021 (1968).
30. R. J. Samuels, *J. Macromol. Sci. (Phys.)*, **B4**, 701 (1970).
31. G. Meinel and A. Peterlin, *J. Polym. Sci. A-2*, **8**, 1723 (1970).
32. G. Meinel, M. Morosoff, and A. Peterlin, *J. Polym. Sci. A-2*, **8**, 1723 (1970).
33. J. J. Hermans, P. H. Hermans, D. Vermeas, and A. Weidinger, *Rec. Chim. Trav.*, **65**, 427 (1946).
34. R. S. Stein, *J. Polym. Sci.*, **31**, 327 (1958).
35. J. L. Matthews, H. S. Peiser, and R. B. Richards, *Acta Cryst.*, **21**, 85 (1949).
36. L. Mandelkern, in *Growth and Perfection of Crystals*, R. H. Doremus, B. W. Roberts, and D. Turnbull, Eds., Wiley, New York, 1958, p. 478.
37. M. Takayanagi and T. Kusumoto, *Kogyo Kagaku Zasshi*, **62**, 587 (1959).
38. J. J. Weeks, *J. Res. Nat. Bur. Stand. A, Phys. Chem.*, **67A**, 441, 1963.
39. W. O. Statton, *J. Polym. Sci.*, **28**, 423 (1958).
40. S. Kavesh and J. M. Schultz, *J. Polym. Sci. A-2*, **9**, 85 (1971).
41. P. Y.-F. Fung and S. H. Carr, *J. Macromol. Sci. (Phys.)*, **B6**(4), 621 (1972).
42. G. R. Taylor and S. R. Darin, *J. Appl. Phys.*, **26**, 1075 (1955).
43. R. J. Samuels, *J. Polym. Sci. A-2*, **10**, 781 (1972).
44. P. H. Geil, *Polymer Single Crystals*, Interscience, New York, 1963, Chap. IV.
45. E. S. Clark and C. A. Garber, *Int. J. Polym. Mater.*, **1**, 31 (1971).
46. R. D. Van Veld, G. Morris, and H. R. Billica, *J. Appl. Polym. Sci.*, **12**, 2709 (1968).
47. E. S. Clark, in *Polymer Science and Technology*, Vol. 1, R. W. Lenz and R. S. Stein, Eds., Plenum Press, New York, 1972.
48. B. S. Sprague, *Bull. Amer. Phys. Soc. II*, **18**, 345 (1973).

Received September 7, 1973